



Two polymorphic cholesterol monohydrate crystal structures form in macrophage culture models of atherosclerosis

Neta Varsano^a, Fabio Beghi^b, Nadav Elad^c, Eva Pereiro^d, Tali Dadosh^c, Iddo Pinkas^c, Ana J. Perez-Berna^d, Xueting Jin^e, Howard S. Kruth^e, Leslie Leiserowitz^f, and Lia Addadi^{a,1}

^aDepartment of Structural Biology, Weizmann Institute of Science, 76100 Rehovot, Israel; ^bDepartment of Chemistry, Università Degli Studi Di Milano, I-20122 Milano, Italy; ^cDepartment of Chemical Research Support, Weizmann Institute of Science, 76100 Rehovot, Israel; ^dMISTRAL Beamline–Experiments Division, ALBA Synchrotron Light Source, Cerdanyola del Valles, 08290 Barcelona, Spain; ^eExperimental Atherosclerosis Section, National Heart, Lung, and Blood Institute, National Institutes of Health, Bethesda, MD 20892-1422; and ^fDepartment of Materials and Interfaces, Weizmann Institute of Science, 76100 Rehovot, Israel

This contribution is part of the special series of Inaugural Articles by members of the National Academy of Sciences elected in 2017.

Contributed by Lia Addadi, June 12, 2018 (sent for review February 20, 2018; reviewed by Bart Kahr and Samuel I. Stupp)

The formation of atherosclerotic plaques in the blood vessel walls is the result of LDL particle uptake, and consequently of cholesterol accumulation in macrophage cells. Excess cholesterol accumulation eventually results in cholesterol crystal deposition, the hallmark of mature atheromas. We followed the formation of cholesterol crystals in J774A.1 macrophage cells with time, during accumulation of LDL particles, using a previously developed correlative cryosoft X-ray tomography (cryo-SXT) and stochastic optical reconstruction microscopy (STORM) technique. We show, in the initial accumulation stages, formation of small quadrilateral crystal plates associated with the cell plasma membrane, which may subsequently assemble into large aggregates. These plates match crystals of the commonly observed cholesterol monohydrate triclinic structure. Large rod-like cholesterol crystals form at a later stage in intracellular locations. Using cryotransmission electron microscopy (cryo-TEM) and cryoelectron diffraction (cryo-ED), we show that the structure of the large elongated rods corresponds to that of monoclinic cholesterol monohydrate, a recently determined polymorph of the triclinic crystal structure. These monoclinic crystals form with an unusual hollow cylinder or helical architecture, which is preserved in the mature rod-like crystals. The rod-like morphology is akin to that observed in crystals isolated from atheromas. We suggest that the crystals in the atherosclerotic plaques preserve in their morphology the memory of the structure in which they were formed. The identification of the polymorph structure, besides explaining the different crystal morphologies, may serve to elucidate mechanisms of cholesterol segregation and precipitation in atherosclerotic plaques.

pathological crystallization | crystal polymorphs | cryo-SXT | STORM | helical crystals

Cholesterol is an essential component of animal cell membranes (1) that regulates the membrane fluidity and mechanical properties.

Cholesterol is continuously supplied to the cells either through synthesis or uptake of exogenous cholesterol, while excess is removed. In this way, a steady equilibrium (cholesterol homeostasis) is achieved. Cholesterol is delivered through the blood to most peripheral tissues by low-density lipoproteins (LDLs), whereas reverse cholesterol trafficking (i.e., removal of excess cholesterol) is mediated by high-density lipoproteins (HDLs) (2). When LDL particles are trapped in the intima, the innermost layer of the artery wall, they may trigger recruitment of monocytes from the blood (3, 4). Within the vessel wall, monocytes differentiate into macrophages that take up large amounts of the trapped LDLs. The accumulated cholesterol is stored in esterified form in cytoplasmic lipid droplets and in unesterified form mostly in lysosomes and cell membranes (5–7). As cholesterol levels increase in the macrophage cell, they become “foam cells,”

and initiate formation of atherosclerotic plaques (8–11). Subsequently, unesterified cholesterol supersaturation in the cells may lead to crystal precipitation, before and/or after cell death (12–14). Crystalline cholesterol is not easily dissolved or removed from the plaques (6). Crystal formation promotes increased inflammatory response, expansion of the necrotic core, and possible plaque disruption, leading to heart attack and stroke (6, 15, 16). Open questions are what triggers crystal formation, what are the biological sites of nucleation, and whether crystallization occurs exclusively at intracellular or extracellular sites.

Cholesterol crystals were observed in atherosclerotic tissues and in cell culture, both in intracellular and extracellular locations (4, 12, 13, 17–19). Two crystal morphologies dominate: elongated rod-like crystals and thin quadrilateral plates (19, 20). The latter are characteristic of the stable triclinic crystals of cholesterol monohydrate (21–23). The triclinic monohydrate crystals (Table 1) are the well-known form deposited in vitro. In gallstones (24, 25), a pathology also related to cholesterol crystal deposition, the triclinic form deposits side by side with a monoclinic cholesterol monohydrate structure (Table 1) (25, 26).

Significance

Atherosclerosis causes heart attack and stroke and is a major fatal disease in the Western world. Cholesterol crystal rods and plates are the hallmark of developed atherosclerotic plaques and are associated with plaque rupture and thrombus formation. We show here that the elongated rod-shaped crystals that form inside macrophage cells enriched with cholesterol have a crystal structure different from the thin plates associated with the cell plasma membrane. The two crystal structures are induced by the different biological environment where they form. Besides identifying the structure of cholesterol crystals in pathological plaques, this work may thus provide information on cellular crystal growth mechanisms, once the factors that favor the formation of the different structures are understood.

Author contributions: N.V., H.S.K., L.L., and L.A. designed research; N.V., F.B., N.E., E.P., T.D., I.P., and A.J.P.-B. performed research; E.P. and X.J. contributed new reagents/analytical tools; N.V., F.B., N.E., E.P., T.D., I.P., L.L., and L.A. analyzed data; and N.V., F.B., H.S.K., L.L., and L.A. wrote the paper.

Reviewers: B.K., New York University; and S.I.S., Northwestern University.

The authors declare no conflict of interest.

Published under the [PNAS license](#).

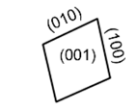
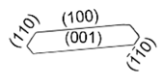
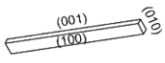
See QnAs on page 7644.

¹To whom correspondence should be addressed. Email: lia.addadi@weizmann.ac.il.

This article contains supporting information online at www.pnas.org/lookup/suppl/doi:10.1073/pnas.1803119115/-DCSupplemental.

Published online July 2, 2018.

Table 1. Cholesterol crystal structure parameters

Crystal	C.S S.G	Unit Cell Dimensions	Crystal Habit	Ref.
Cholesterol monohydrate $C_{27}H_{46}O \cdot H_2O$	Triclinic P1	$a = 12.39 \text{ \AA}, b = 12.41 \text{ \AA}, c = 34.36 \text{ \AA}$ $\alpha = 91.9^\circ, \beta = 98.1^\circ, \gamma = 100.8^\circ$		22
Cholesterol monohydrate $C_{27}H_{46}O \cdot H_2O$	Monoclinic A2	$a = 10.15 \text{ \AA}, b = 7.57 \text{ \AA}, c = 68.2 \text{ \AA}$ $\beta = 94.8^\circ$		30
Anhydrous cholesterol $C_{27}H_{46}O$	Triclinic P1	$a = 14.17 \text{ \AA}, b = 34.21 \text{ \AA}, c = 10.48 \text{ \AA}$ $\alpha = 94.64^\circ, \beta = 90.67^\circ, \gamma = 96.32^\circ$		28

C.S, crystal system; S.G, space group.

The rod-like crystals have the morphology of cholesterol in the anhydrous form (27, 28) and were indeed suggested to have the structure of anhydrous cholesterol (Table 1) (12). Studies performed on fresh samples from atherosclerotic plaques, however, proved that no cholesterol crystals in the anhydrous form existed in the plaques examined (21, 23, 29). The presence of two distinct morphologies appears to indicate that the crystals formed in a different environment, possibly intracellular and extracellular.

The 3D cholesterol monohydrate crystals form spontaneously from 2D ordered cholesterol domains in compressed cholesterol monolayers and multilayers (30, 31). Similar 3D cholesterol crystal nucleation from segregated cholesterol domains occurs in phospholipid/cholesterol bilayer mixtures, beyond a critical local cholesterol concentration (32, 33).

Based on this work, and on work performed on macrophage cells enriched with cholesterol, we suggested that cholesterol crystal nuclei may form from segregated 2D microdomains in the cell plasma membrane, in an early stage of the atherosclerotic plaque progression (33, 34).

We demonstrated *in vitro* that under high cholesterol levels in supported lipid bilayers, 2D cholesterol membrane domains may serve as nucleation sites for the formation of 3D cholesterol monohydrate crystals (35). To verify whether similar crystallization events may be relevant to crystal formation in cells, we developed a correlative method that combines cryosoft X-ray tomography (cryo-SXT) with stochastic optical reconstruction microscopy (STORM) (36). The binding to an antibody that specifically recognizes cholesterol ordered arrays (37, 38) identifies the crystals (by STORM), while 3D imaging of the cell components using cryo-SXT reveals their locations.

The STORM/cryo-SXT correlative approach was applied to murine RAW267.4 macrophage cells. After 48-h incubation with acetylated LDL particles (acLDLs), thin quadrilateral cholesterol crystal plates of size as small as 200 nm were identified. These were located in close association with the cell plasma membrane (36).

Human monocyte-derived macrophages, grown under the same cholesterol accumulation conditions, develop cholesterol ordered domains in the plasma membrane (34, 39, 40), although it is not known yet whether they develop 3D crystals. However, mouse peritoneal macrophages (MPMs) as well as J774A.1 macrophages produce large intracellular needle-like (or rod-like, as we shall refer to in this work) crystals, similar in morphology to those isolated from human plaques (12, 13, 20).

Macrophage cultures, in particular from the J774A.1 cell line, are widely used in cell culture models of atherosclerosis, and the pathways of cholesterol accumulation are relatively well characterized (4, 8, 13). Here, we followed the formation of

cholesterol crystals in J774A.1 macrophage cells with time, during uptake of acLDL particles and enrichment of the macrophages with cholesterol.

Results

To follow cholesterol crystal formation, we used the same 3D correlative approach combining STORM with cryo-SXT that we developed for RAW264.7 cells (36). Briefly, macrophage J774A.1 cells were grown on gold *finder*-grids and were incubated with acLDL for 24, 36, or 48 h. After fixation, the cells were fluorescently labeled with the structural monoclonal antibody (mAb) 58B1 that recognizes cholesterol 2D and 3D crystals (37, 38), and the fluorescence was recorded with STORM at an *xy* resolution of ~30 nm and a *z* resolution of ~80 nm. The grids were then vitrified and imaged by using SXT (41). Tomograms were taken from the same cells that were analyzed by STORM, and the reconstructed volume was overlaid on to the STORM 3D data following the correlative workflow described in figure 4 of ref. 36, our recent study. For more details on the data alignment, see *SI Appendix, SI Materials and Methods*.

Plate Crystals Associated with the Cell Plasma Membrane. The projected and superimposed 3D data of cells after 24-h incubation with acLDL showed a STORM sporadic dot pattern that covered most of the cell plasma membrane (Fig. 1*A* and *B*).

The sporadic dot pattern corresponds to 2D crystalline domains of cholesterol that form in cell membranes (34, 39). Few of the domains assemble into larger clusters (>200 nm), which are juxtaposed with the cell plasma membrane (Fig. 1*A* and *B*, arrows, schematics in Fig. 1*C*). Observation from the relevant perpendicular plane (Fig. 1*D*, slice profiled in light blue) shows that the larger clusters colocalize with distinct sharp features imaged by cryo-SXT (Fig. 1*D*, arrows, Fig. 1*E–H*). The SXT shapes of the STORM-labeled features have sizes of 500–700 nm and a quadrilateral morphology (Fig. 1*E–H*) that corresponds to that of 3D cholesterol monohydrate crystals in the stable (triclinic) form (Table 1). Smaller crystals, with sizes 200–300 nm, were also detectable (Fig. 1*I–L*). Smaller domains of 30–100 nm did not unequivocally colocalize with recognizable morphologies in SXT.

Interestingly, an additional labeling pattern appeared occasionally after 24-h incubation with acLDL and became progressively more frequent after 36- to 48-h incubation. This pattern was characterized by isolated large signal concentrations (size range of 1–3 μm) (Fig. 2*A* and *B*, arrows). The STORM localization map in Fig. 2 shows two such large signal concentrations located at two different heights on the cell plasma membrane (Fig. 2*B*). High magnification of the overlaid 3D correlative map revealed that the large signal foci are aggregates

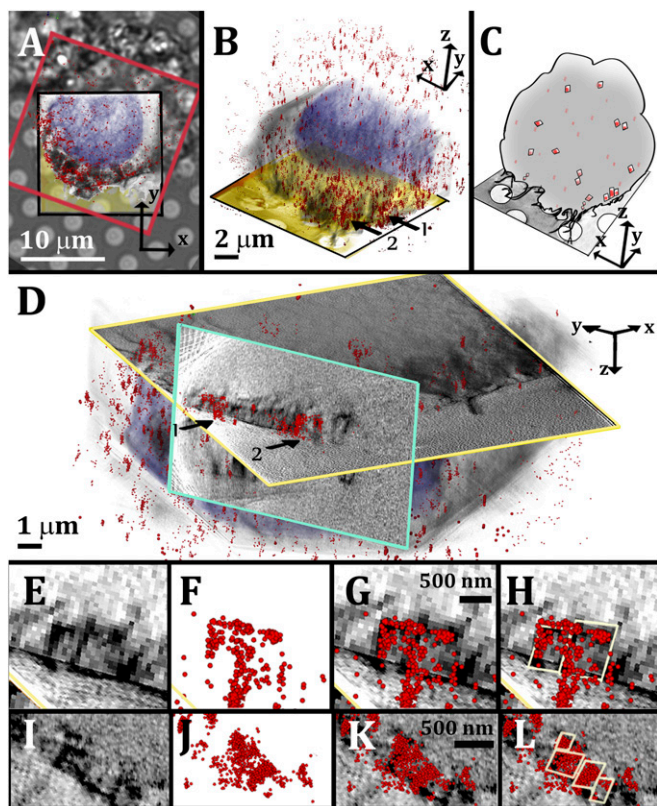


Fig. 1. Correlative STORM/cryo-SXT imaging of 3D cholesterol crystals associated with cell membranes. (A) Superimposition of a bright-field image of a cell with the corresponding STORM data (red frame) and the 3D volume rendering of the SXT segmented data (black frame). The different features of the STORM and SXT are highlighted using arbitrary colors: STORM localization map, sporadic red dots; cell nucleus, blue-purple; and cell volume, gray. The grid foil is colored in yellow in the slice through the 3D reconstruction of the cell tomogram. (B) The 3D overlaid SXT and STORM segmented data of the same cell, from a side view. Features labeled with arrow 1 are followed in D–H and features labeled with arrow 2 in D. (C) Cartoon rendering of the overlaid data in B. (D) Slices through the reconstructed SXT data used to visualize the crystal profiles identified by STORM. The xy slice (profiled in yellow) is combined with a perpendicular slice (profiled in light blue). (E and I) SXT of two different groups of crystals with quadrilateral profile. (F and J) Corresponding STORM data. (G and K) Superimposition of STORM and SXT. (H and L) The profiles of the crystals are marked in yellow for easier visualization. This was performed manually, based on the SXT contrast.

composed of smaller clusters that colocalize with quadrilateral features imaged by cryo-SXT (Fig. 2 D–G and *SI Appendix*, Fig. S1). We interpret these features as assemblies of triclinic crystal plates packed together without any particular order or orientation (schematics in Fig. 2C).

While the earlier observations were indicative of a possible nucleation and growth process of cholesterol in membranes, this latter observation may correspond to a different stage of crystal aggregation that becomes more common at longer incubation times.

We applied STORM to the sequence of events of cholesterol phase separation from lipid mixtures in the cell membranes. Several batches of macrophage J774A.1 cells were incubated with or without acLDL for different times, ranging between 10 and 48 h. Cells were then fixed, fluorescently labeled with the structural antibody mAb 58B1, and imaged both in wide field and with STORM. The superresolution signal was recorded from the entire volume of the cells, at each time point (2,000 frames from multiple z positions using 1- or 0.5- μm steps).

The wide-field fluorescence intensity of control cultures incubated without acLDL was minimal (*SI Appendix*, Fig. S2A) and was set as reference for normalization of the subsequent data within the same batch ($t = 0$ h, Fig. 3A). The fluorescence intensity increased with increasing acLDL incubation times (Fig. 3A), reflecting the emergence of cholesterol ordered areas labeled by antibody 58B1. After 24 h, the labeling intensity was already three times higher than the control (Fig. 3A). The domain areas were then analyzed for each incubation time point by using the Vutara SRX cluster analysis software (more details are in *SI Appendix*, *SI Materials and Methods*). The average area in xy plane projections of labeled domains increased with time (Fig. 3 B and C–F, *Insets*) whereas the number of overall labeled domains did not necessarily increase (*SI Appendix*, Fig. S2B).

Labeled crystalline domains at short incubation times (10 h) are characterized by narrow size distribution and have a typical area of 1×10^3 to 5×10^3 nm^2 (Fig. 3B), corresponding to approximate lateral sizes of 30–70 nm. Note that domains that predominantly extend in the z direction have effective areas much larger than their projections in the xy plane. At this time

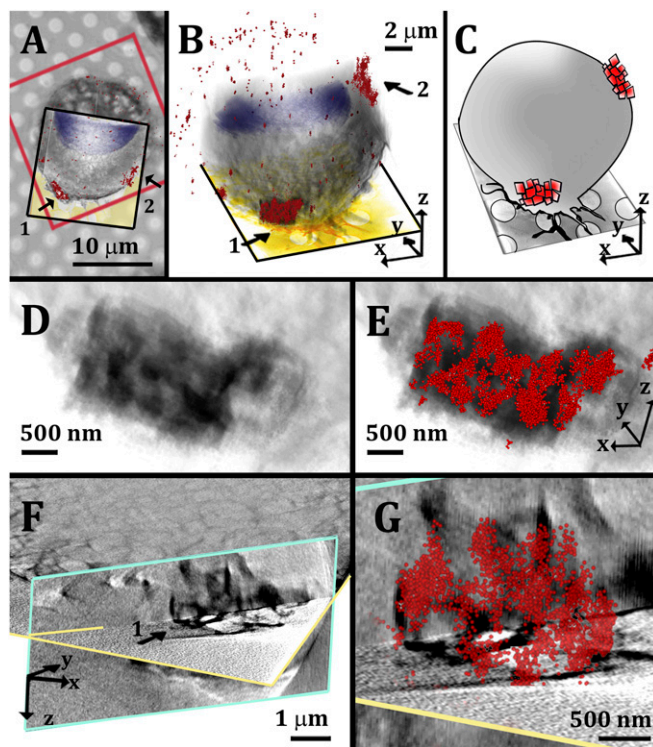


Fig. 2. Correlative STORM/cryo-SXT imaging of micrometer-size cholesterol crystal aggregates associated with cell membranes. (A) Superimposition of a bright-field image of a cell with the corresponding STORM data (red frame) and the 3D volume rendering of the SXT segmented data (black frame). The different features of the STORM and SXT are highlighted using arbitrary colors: STORM localization map, red clusters 1 and 2; cell nucleus, blue-purple; cell volume, gray. The grid foil is colored in yellow in the slice through the 3D reconstruction of the cell tomogram. (B) The 3D overlaid SXT and STORM segmented data of the same cell, from a side view. Cluster labeled with arrow 1 is followed from D to G. (C) Cartoon rendering of the overlaid data in B. (D) High magnification of the segmented volume of aggregate 1 in approximately the same orientation as in B. (E) The same volume as in D superimposed with the corresponding STORM data (red). (F) Slices through the reconstructed SXT data used to visualize the crystal profiles identified by the cluster in STORM. The xy slice (profiled in yellow) is combined with a perpendicular slice (profiled in light blue). (G) High magnification of aggregate 1 in F, superimposed with the corresponding STORM data (red).

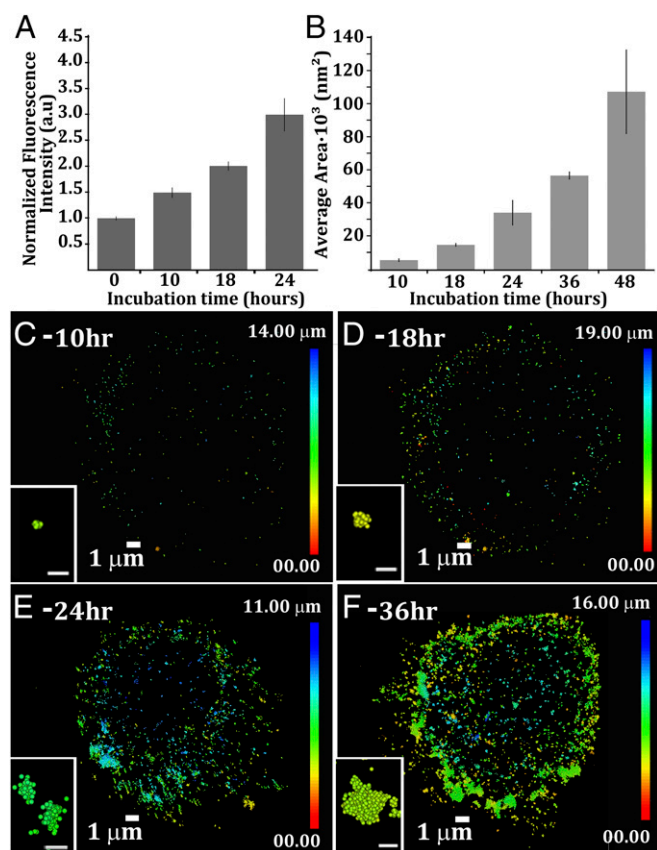


Fig. 3. Time evolution of plasma membrane crystalline cholesterol domains. (A) Time course of segregated cholesterol domain growth. Data were analyzed for average pixel intensity from the wide-field fluorescence images. The starting point ($t = 0$) corresponds to cells that were not incubated with acLDL. The fluorescence level at $t = 0$ was assigned to 1, and the subsequent measurements were normalized to this level. Data are normalized mean ($n = 10$) \pm SE. (B) Average cluster area after different incubation times with acLDL (mean \pm SE; $n = 3-6$). Data were analyzed by using the Vutara SRX statistical package. (C–F) Resolved superresolution localization map after different incubation times with acLDL (C, 10 h; D, 18 h; E, 24 h; F, 36 h). *Insets* show high magnifications of representative clusters in the STORM data from a top view. [Scale bars (*Insets*): 100 nm.] The color scales indicate the heights of the domains in the cell: blue, top of the cell; red, bottom of the cell.

point, the crystalline domains in the STORM reconstructed 3D localization map are small clusters that mostly localize at the outer rim of the cell and have no detectable morphology (Fig. 3C, *Inset*). At 18 h, the domain areas cluster around $15 \times 10^3 \text{ nm}^2$, $\sim 120 \text{ nm}$ in lateral size, and they grow to an average projected area of $35 \times 10^3 \text{ nm}^2$, corresponding to $\sim 190 \text{ nm}$ in lateral size (Fig. 3B). At 24 h, domains spread all over the cell surface, and several have, even in the xy projection, a typical quadrilateral shape (Fig. 3E, *Inset*). They correspond to the 3D images of crystals in Fig. 1 I–L. After 36-h incubation with acLDL, the average area of the domains increased to $60 \times 10^3 \text{ nm}^2$, corresponding to $\sim 250 \text{ nm}$ in lateral size in projection, and further increases to $>100 \times 10^3 \text{ nm}^2$ ($>320 \text{ nm}$ projected lateral size), at 48 h (Fig. 3B). The STORM localization maps show large labeling foci (Fig. 3F, *Inset*) that likely correspond to the packed crystal aggregates in Fig. 2. As incubation time increases, the population of the small cholesterol domains decreases (SI Appendix, Fig. S3). The decrease in the small domain populations is coupled with the increase in the large domain population and with a wider size diversity.

These results indicate a progression of cholesterol accumulation, whereby cholesterol initially phase separates in the cell

membranes to form small domains with relatively uniform sizes. The domains subsequently grow into plasma membrane-associated crystals, and then assemble into crystal aggregates.

Note that these observations refer predominantly to cholesterol segregated in the plasma membrane. The STORM signal is associated with antibody binding, and the antibodies do not have free access into the cell. The-SXT transmitted signal has also limited possibility of intracellular imaging in fixed cells, due to increased absorption of the signal intrinsic to the fixation.

Large Rod-Like Crystals. Long incubation of J774A.1 cells with acLDL ($\geq 30 \text{ h}$) induced the formation of large 3D features that are visible by light microscopy and were identified as crystals by polarized light (Fig. 4 A–D). The crystal morphology was rod-like, with a long axis of a few tens of micrometers. The crystals were always observed at intracellular locations and appeared to be “piercing” the cell plasma membrane from the inside (Fig. 4). Some of the crystals appeared curved (Fig. 4C) and were dimmer between crossed polarizers (Fig. 4D). There was no evidence under our experimental conditions that crystals grew outside cells and ultimately underwent phagocytosis.

To verify that these were indeed cholesterol crystals, the cells were examined by STORM and cryo-SXT following the correlative approach described above (e.g., Fig. 4 E–J). Slices through the reconstructed 3D data confirmed that the crystal in Fig. 4 E–I was indeed located inside the cell volume (Fig. 4G). The crystal appeared as crossing the cell volume, emerging from the two sides of the cell, although on the left side of the image, the crystal was still covered by the cell membrane (Fig. 4 H and I). Other crystals were completely enclosed by the cell and had no obvious association with the cell plasma membrane (SI Appendix, Fig. S4).

Needle or rod-like morphology is not typical of triclinic cholesterol monohydrate crystals which, when crystallized from aqueous solutions, appear as quadrilateral plates (6, 22, 27). The observation of elongated crystals thus raises the possibility that this is a different form of crystalline cholesterol. The elongated morphology is consistent with anhydrous cholesterol, but micro-Raman spectroscopy performed in situ on the cultured cells ruled out this possibility. The Raman spectra corresponded to a monohydrate structure (SI Appendix, Fig. S5).

Unequivocal identification of the crystal structure of the rod-like crystals was obtained by cryoelectron diffraction (cryo-ED). Cells were grown directly on carbon-coated gold grids, enriched with acLDL for 48 h, and vitrified. The grids were plunge-frozen and analyzed by using cryotransmission electron microscopy (cryo-TEM) in imaging and electron diffraction (ED) modes.

Several crystals were observed emerging from cells, but only few of these were thin enough to yield clear ED patterns. Fig. 5A1 presents one such specimen. The diffraction pattern (Fig. 5A2) exhibits Laue mm symmetry, with several intense but streaked reflections, and one clear lattice spacing of 7.5 \AA . This observed Laue mm symmetry was perplexingly higher than that of the triclinic anhydrous and monohydrate phases.

Besides the anhydrous cholesterol form, there are two known monohydrate polymorphs of cholesterol crystals formed from water (Table 1): The crystal and ED pattern of the stable triclinic form are reported in SI Appendix, Fig. S6, and the simulated ED patterns of the recently discovered monoclinic form are reported in SI Appendix, Fig. S7 (30, 31).

The ED pattern of a well-formed cholesterol crystal in the monoclinic polymorph is shown in Fig. 5B. The crystal grew in vitro from a supported lipid bilayer composed of 42:18:40 mol% cholesterol/ 1,2-dipalmitoyl-sn-glycero-3-phosphocholine (DPPC)/ 1-palmitoyl-2-oleoyl-sn-glycero-3-phosphocholine (POPC), externally supplemented with cholesterol (35). The ED pattern of the elongated crystal in Fig. 5B exhibited Laue mm symmetry, with 7.5- and 10- \AA lattice spacings along the b^* and a^* directions.

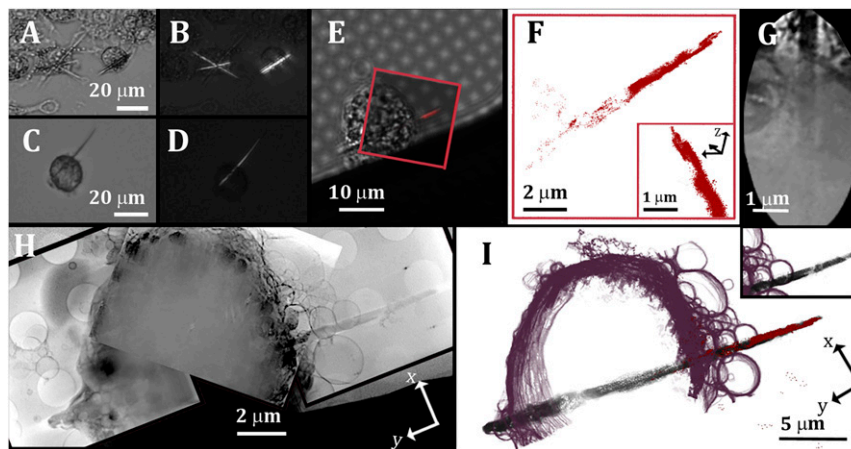


Fig. 4. Rod-like cholesterol crystals after extended macrophage enrichment with acLDL. (A and C) Bright-field images of cells following 36-h incubation with acLDL. Several cells contain crystals that are tens of micrometers long. (B and D) Photomicrographs of the same microscopic fields as in A and C taken with crossed polarizers. (E) Bright-field image of a cell following incubation with acLDL, fixation, and antibody 58B1 labeling, overlaid with the corresponding fluorescence data (red). The antibody labels only the extracellular portion of the crystal, because it does not have easy access into the cell. (F) Localization map of the resolved STORM data (red spots) of the crystal (xy plane) and from side view in *Inset*. (G) High magnification of a detail in the reconstructed X-ray data showing the cell membrane where the crystal emerges and part of the crystal inside the cell volume. The extracellular part of the crystal is clear in the top part of the image, whereas the intracellular part is dimly outlined because of the high density of the cell. (H) Mosaic of three slices through the combined 3D reconstruction tomograms of the same cell presented in E (xy plane). (I) The 3D X-ray segmented data superimposed with the STORM signal (red). The different features are segmented using arbitrary colors: plasma membrane, purple; cholesterol crystal, black-gray. (I, *Inset*) Segmented data of SXT only.

The 7.5-Å spacing measured in Fig. 5A2, together with the symmetry of the diffraction pattern, provides fingerprint evidence that the crystal in Fig. 5A1 belongs to the monoclinic form of cholesterol monohydrate. The crystal habit extends along the b axis. We interpreted the “streakiness” of the diffraction spots along the a^* axis, together with the absence of the low-order $h00$ and $11l$ diffraction peaks, as being due to the folding of the crystal around the b axis. This is further elaborated upon below. The transmission image in fact (Fig. 5A1) shows a reduced contrast in the central part of the specimen and at one ending part of the crystal, indicative of a tube-like shape.

Cholesterol crystals grown in vitro from lipid bilayers also occasionally appear as tube-like fibers with decreased contrast in the central part of the fiber (Fig. 5C1). The diffraction patterns from these fibers comprise the telltale spacing of 7.5 Å (b axis) between rows of intense, blurred spots exhibiting (hk) l satellites, varying in the l index on the horizontal line (Fig. 5C2). The spacing between the satellite spots is ~ 36 Å, near to the 34.1 Å $d(002)$ spacing along the c axis, when taking into account the deformation of the spots. The diffraction pattern is a superposition of the diffraction patterns of the monoclinic structure viewed along $[001]$ and $[100]$ (Fig. 5C2). This superimposition results from the tubular morphology of the crystal. When the electron beam strikes the tube wall edge-on, the a axis is parallel to the electron beam, and so the $0kl$ reflections are in diffraction mode, whereas when the beam strikes the tube wall face-on, the c -axis is parallel to the electron beam, and thus the $hk0$ reflections are in diffraction mode. The blurring of the spots may arise from the curvature, combined with c^* being short, causing many reflections to appear simultaneously (SI Appendix, Fig. S7) (30, 42). The tube grows along the crystallographic b axis and curves along the a axis.

The volume rendering of one of the crystals imaged by SXT in the correlative mode also shows a tubular morphology with decreased contrast in the central part (Fig. 5D), similar to the crystals in Fig. 5A1 and C1.

A different diffraction pattern was measured from the crystal in Fig. 6A. The revealing feature in the diffraction pattern was the 35-Å lattice spacing, corresponding to half the length of the c axis in monoclinic cholesterol monohydrate. Surprisingly, a

magnified TEM image revealed a helical ribbon (Fig. 6A2 and A3). We note that similar helical ribbon cholesterol crystals grow in bile acid environments (26).

The best fit of the ED data to the monoclinic structure was obtained considering that the incident beam is perpendicular to the interlayer c^* axis and to the $[\bar{1}20]$ axial direction. We interpreted these data as describing a ribbon coiling around the $[\bar{1}20]$ direction, with the 35-Å spacing corresponding to the bilayer recurrence across the thickness of the ribbon (should be 34.1 Å), and the 4.5 Å corresponding to slightly distorted $21l$ spacings (should be 4.2 Å) (Fig. 6A4). The strong spots in the middle of the pattern fit the 004 and 0012 reflections. The $21l$ diffractions with intensities matching those obtained here were observed from crystalline cholesterol multilayers (SI Appendix, Fig. S8) (30). The ribbon grew along the b axis as in the tubular crystals in Fig. 5A and C. The $[\bar{1}20]$ coiling axis direction comes from the b axis forming an angle of 34° with the crystallographic axis b . The model is presented in Fig. 6B.

Other crystals growing from the macrophage cells, and which we observed with SXT, had thicknesses within the range of 0.5–1 μm . These crystals are likely too thick to provide an ED pattern. Under renewed consideration of the SXT data, however, we observed that the volume rendering of several segmented crystals showed that they have helical morphology, in agreement with the crystal in Fig. 6A (Fig. 6C–F).

Discussion

In this study, we characterized different stages of cholesterol segregation in J774A.1 macrophage cells and identified two cholesterol monohydrate crystal morphologies. Small-quadrilateral plate crystals, associated with cell plasma membranes, were detected at early stages of cholesterol accumulation. Intracellular rod-like crystals, which often cross the cell from side to side, were detected at relatively advanced stages of cholesterol accumulation. The rod-like crystals were characterized as cholesterol monohydrate with monoclinic symmetry. This work provides an unequivocal identification of monoclinic cholesterol monohydrate crystals in atherosclerosis-related models.

A time evolution study showed that cholesterol crystalline domains form in membranes of J774A.1 macrophages at early

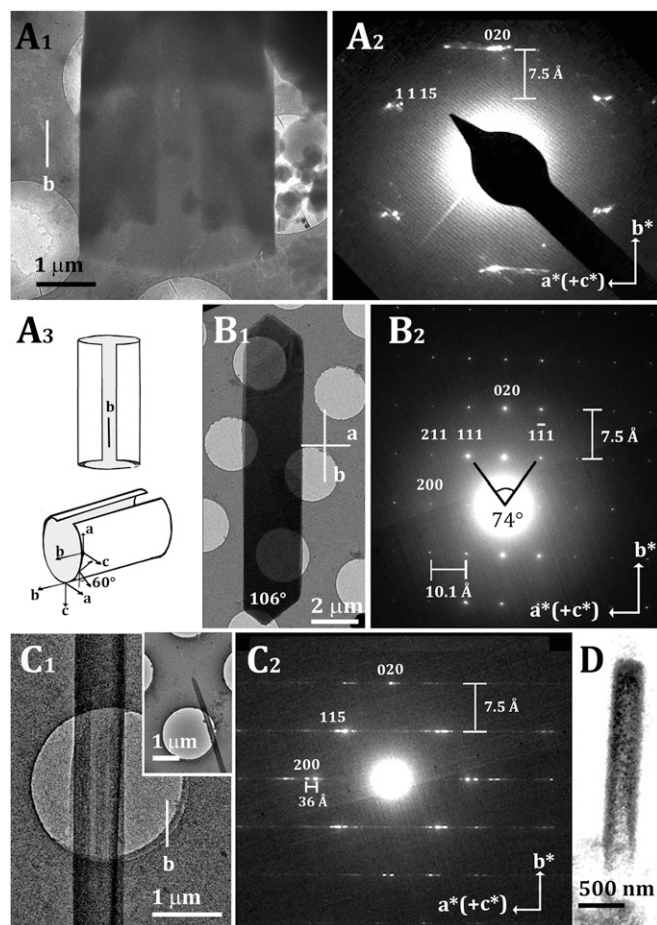


Fig. 5. Cryo-TEM and ED of cholesterol crystals grown in cells and on lipid bilayers. (A) Cryo-TEM image and diffraction of a cholesterol crystal grown in a cell following incubation with acLDL for 48 h. (A1) Cryo-TEM image. (A2) Cryo-ED pattern. The two blurred spots on the central axis correspond to 020 and 020. The 1,1,15 reflection implies an angle of 60° between the *c* axis and the incident beam, suggesting an elliptical cross section of the tube (A3). (A3) Proposed open-tube model of the crystal in A1 and A2. The direction of the *b* axis remains constant, whereas the direction of the *a* axis rotates with the tube curvature. (B) Faceted monoclinic cholesterol monohydrate crystal grown on a supported lipid bilayer composed of cholesterol/DPPC/POPC = 42/18/40 mol%, externally supplemented with cholesterol. (B1) Cryo-TEM image. (B2) Cryo-ED pattern. (C) Tubular cholesterol crystal grown on a supported lipid bilayer as in B. (C1) Cryo-TEM image. (C1, Inset) The same crystal at low magnification. (C2) Cryo-ED pattern. (D) Volume rendering of the segmented cryo-SXT data of a crystal from one cell, grown under the same conditions as the cells in Figs. 4 and 6, showing tubular morphology.

stages of cholesterol accumulation. The overall size of these cholesterol domains increases with incubation time, reaching a size-range of hundreds of nanometers. Already at a very small size, the domains assume a plate habit typical of crystalline cholesterol monohydrate in the triclinic structure, the phase known to accumulate in the disease (6, 23). Using correlative cryo-SXT/STORM, we show that the 3D cholesterol crystals are associated with the cell plasma membrane, surrounded by membrane-embedded cholesterol crystalline domains.

Such plate-shaped cholesterol crystals form also from the cell plasma membrane of RAW267.4 macrophages (36). The observation made now in J774A.1 cells expands the scope of the result to different macrophage cell lines and supports the hypothesis that cholesterol nucleation from cell membranes is a process not restricted to specific biological conditions existing only in certain types of macrophages.

Kellner-Weibel et al. (12) studied cholesterol crystal formation from J774A.1-cholesterol loaded cells. Several tens-of-micrometer-large plate-shaped crystals with cholesterol monohydrate triclinic structure were observed in the extracellular space, after stimulation of cholesterol ester hydrolysis and inhibition of cell growth. Our results support the possibility that also in this case crystal nucleation occurred at cell membranes, as suggested (12). It is possible that undetected nanometer-size crystals, associated with the plasma membrane, formed even before treatment.

As more cholesterol accumulates in the macrophage cells, the population of plate-crystals in the membrane increases, together with the formation of micrometer-size aggregates of smaller plate crystals. This type of crystal aggregates may be the result of an active mechanism, where the cell packs the small 3D crystalline cholesterol plates for secreting them to the extracellular space and in this way restores membrane flexibility.

Incubation times >30 h give rise to sparse formation of long and thin rod-like cholesterol crystals inside the cell. The rod-like crystal morphology is suggestive of a different crystal growth pathway. We did not find any indication of anhydrous cholesterol, consistent with failed attempts to document such crystals in tissue sections (23, 29) or in model cell cultures (12).

The rod-like crystals analyzed here by ED consist of the monoclinic cholesterol monohydrate phase, a recently discovered cholesterol monohydrate polymorph (30, 31). This polymorph was first determined from cholesterol multilayers (30, 31) and was later observed to form from supported ceramide/cholesterol lipid bilayers (33) and from DPPC/cholesterol lipid

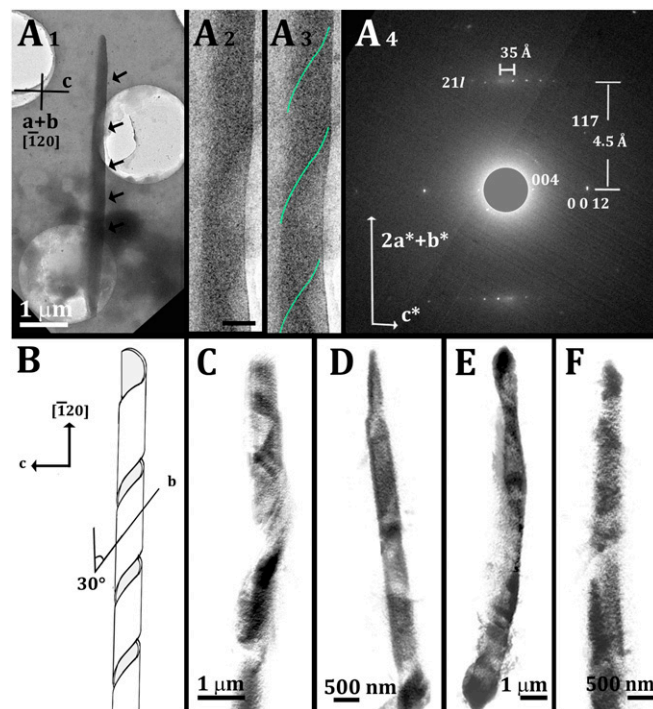


Fig. 6. Cryo-TEM and cryo-SXT of helical cholesterol crystals grown in cells. (A) Cryo-TEM image and diffraction of a cholesterol crystal grown in a cell following incubation with acLDL for 48 h. (A1) Cryo-TEM image. The arrows indicate notches that are barely visible at this low magnification. (A2 and A3) High magnification of the central part of the crystal, with the notches clearly visible: The crystal consists of a helical ribbon; a green line marks the coils in A3 for ease of recognition. (Scale bar: 500 nm.) (A4) Cryo-ED pattern of the crystal in A1–A3. The direct beam was masked to allow easier detection of the 004 diffraction spots. (B) Proposed helical coil model. (C–F) Volume rendering of the segmented cryo-SXT data of four different crystals from several cells, showing helical coiled morphology.

bilayers, externally supplemented with cholesterol (35). The structures of both monohydrate polymorphs feature cholesterol bilayers interleaved with water molecules bound to the cholesterol hydroxyl groups and are in general very similar. The water molecule hydrogen-bonding pattern and the interactions between cholesterol molecules are, however, different in the direction of the crystallographic *b* axis (Table 1). This may well be the reason why the triclinic polymorph grows as quadrilateral plates, whereas the monoclinic polymorph grows as long thin ribbons. The weak interactions between the hydrophobic side chains of cholesterol molecules juxtaposed in successive bilayers explain why the ribbons are thin. It is not clear why the thin ribbons fold either as cylinders or as helices, although other molecular crystals also bend, twist, and fold into helices during growth (43–46).

The relevance of the monoclinic cholesterol crystals to human pathological cases was first reported in relation to cholesterol crystallization in bile (26). In the bile system, the monoclinic crystals were identified as a metastable precursor that eventually transforms into the known triclinic monohydrate polymorph (25). Both structures coexist in most of the crystallization stages from model bile and from native bile (25, 26).

Konikoff et al. (47) also showed that different phospholipid mixtures can induce different cholesterol superstructures. Saturated phospholipids preferentially follow the “plate-like crystal pathway,” whereas very short or unsaturated lipids induce the formation of “spirals, helical ribbons and tubes.”

It is known that the lipid composition varies between the plasma membrane and other cellular membranes, with saturated lipids and sphingolipids being more abundant in the cell plasma membrane. We consequently speculate that the crystallization of the monoclinic rods in J774A.1 macrophages may occur from a different cellular lipid environment than that in the plasma membrane.

Interestingly, Kellner-Weibel et al. (12) observed mysterious elongated helices associated with MPM cells, side by side with needle-like crystals, although the nature of the helices was not investigated. Tangirala et al. (13) suggested that the large rod-like crystals observed inside the J774A.1 cells nucleate from secondary lysosomal compartments.

In view of all of the above considerations, we suggest the following scenario: Incubation with acLDL induces an increase in cholesterol concentration in the cell compartments and, in particular, in the cell plasma membrane. The physiological cholesterol concentration is higher in the plasma membrane than in all other cell membranes because of the large concentration of sphingolipids, such as sphingomyelin, for which cholesterol has high affinity (48). When the increased cholesterol concentration overcomes saturation [cholesterol/phospholipid > 1/1 (48)], cholesterol domains segregate, eventually giving rise to the formation of triclinic cholesterol monohydrate plates. This observation is in agreement with the predominant growth of cholesterol monohydrate crystal plates *in vitro* from lipid bilayers containing cholesterol and sphingomyelin (35). When the macrophage cells are supplemented with even higher concentration of cholesterol, large amounts of cholesterol accumulate in the cell membranes, lipid droplets, and lysosomal compartments (5, 6, 8). This results in crystallization in other cell locations besides the plasma membrane, such as in lysosomes. At this later stage, crystals form as large rods that we have now identified as monoclinic cholesterol monohydrate. It was recently shown that inhibition of different cellular pathways may alter cholesterol crystal morphology (19). Specifically, different forms of cholesterol storage within lysosomes or in lipid droplets lead to the formation of either plate or needle crystals. If the elongated crystals form from lipid droplets, it is conceivable that they crystallize by epitaxy from long-chain cholesterol ester bilayers, incorporating the distinctive $10 \times 7.5\text{-\AA}^2$ motif of the monoclinic structure.

Cholesterol monohydrate crystals are found in extensive amounts in necrotic cores of atheroma lesions taken from

humans and animal models. Crystallographically, they correspond to the triclinic structure (6, 21, 23). Histologically, the crystals in atherosclerotic plaques appear as needles (6, 16, 49), although their exact morphology may be difficult to determine. The clefts left by the dissolved crystals appear as needles in TEM as well (13, 17, 18, 50). Admittedly, this observation may be, as suggested, the result of a cross-section through thin plates (6). However, two distinct cholesterol crystal morphologies, plates and rods, were isolated from human atherosclerotic plaques and were clearly detected by light microscopy (20).

Our results indicate that the plates and rods observed in atheromas may correspond to the two different monohydrate polymorphs. We do not know what the conditions under which the rod-shaped crystals form in the plaque are. We do suggest, however, that these morphologies are testimony of formation of the crystal in the monoclinic structure. Even if, at a later stage, the crystal structure transforms into the more stable triclinic polymorph, the morphology of the mature crystals preserves the imprint of the monoclinic polymorph. The transformation may occur at any time during plaque maturation. A single-crystal to single-crystal transformation that preserves crystal morphology is likely, because the molecular rearrangement required is minor. The mechanism would involve a rotation of half of the cholesterol molecules around their molecular axis in a molecular layer, followed by a minor shift of molecular rows within the layer (30, 31).

The structural differences between the two polymorphs and their relation to crystal morphology may now open the path for an investigation, at the molecular level, of cholesterol nucleation and growth. Once the factors that favor the formation of the monoclinic polymorph are understood, mechanistic information on the cellular pathways of cholesterol crystal formation may become evident. To this aim, it is necessary to establish the relative stability of the two different crystalline polymorphs experimentally in different environments and by lattice computations.

Concluding Remarks

The observation that cholesterol crystals form in two different polymorphic phases in J774A.1 macrophages supplemented with excess cholesterol indicates two different formation mechanisms probably triggered by the different environments of the nucleation sites. Crystals formed in association with the plasma membrane assume the triclinic polymorph structure and plate morphology, whereas crystals formed intracellularly assume the monoclinic polymorph structure and elongated morphology. The crystal morphology is thus an informative tool in the study of crystal-formation mechanisms under different conditions or treatments in cell culture. The crystal morphologies of the two polymorphs correspond to those observed in atherosclerotic plaques. We suggest that the rod-like crystals isolated from atheromas derive from a memory of the crystals having formed in the monoclinic structure, and possibly phase-transformed to the triclinic structure over long periods. If this is indeed the case, investigation of the relative distribution of the two morphologies in the plaques may provide information on the crystal nucleation environment and eventually on the mechanisms of crystal formation.

Materials and Methods

Correlative Cryo-SXT/STORM. All of the procedures for the correlative measurements, including antibody purification, cell culture, immunolabeling, STORM imaging, and cryo-SXT, were reported in ref. 36 and are further described in *SI Appendix, SI Materials and Methods*.

Cryo-TEM for ED. Cells were cultured on gold quantifoil TEM grids and incubated with acLDL for 48 and 36 h, plunge-frozen into liquid ethane, and observed with an FEI Tecnai T-12 transmission electron microscope operating at 120 kV or with an FEI Tecnai F-20 TEM operating at 200 kV under low-dose conditions.

Supported lipid bilayers were prepared following the vesicle fusion procedure as described in refs. 33 and 35. Vesicles were deposited on the grids, plunge-frozen, and examined as described above for the cells. Detailed

descriptions of the techniques used are reported in *SI Appendix, SI Materials and Methods*.

Raman Spectroscopy. Cells were cultured on glass-bottom culture dishes and examined in a hydrated condition with a LabRAM HR Evolution instrument (Horiba) configured with four laser lines (325, 532, 632, and 785 nm), allowing for Raman spectra from 50 cm^{-1} onward. Details are in *SI Appendix, SI Materials and Methods*.

- Alberts BJA, Lewis J, Raff M, Roberts K, Walter P (2002) *Molecular Biology of the Cell*, 4th Ed. (Garland, New York).
- Rosenson RS, et al. (2012) Cholesterol efflux and atheroprotection: Advancing the concept of reverse cholesterol transport. *Circulation* 125:1905–1919.
- Gerrity RG (1981) The role of the monocyte in atherogenesis: I. Transition of blood-borne monocytes into foam cells in fatty lesions. *Am J Pathol* 103:181–190.
- Kruth HS (2001) Macrophage foam cells and atherosclerosis. *Front Biosci* 6:D429–D455.
- Jerome WG, Lewis JC (1987) Early atherogenesis in the White Carneau pigeon. III. Lipid accumulation in nascent foam cells. *Am J Pathol* 128:253–264.
- Small DM (1988) George Lyman Duff memorial lecture. Progression and regression of atherosclerotic lesions. Insights from lipid physical biochemistry. *Arteriosclerosis* 8:103–129.
- Brown MS, Goldstein JL (1983) Lipoprotein metabolism in the macrophage: Implications for cholesterol deposition in atherosclerosis. *Annu Rev Biochem* 52:223–261.
- Tangirala RK, Mahlberg FH, Glick JM, Jerome WG, Rothblat GH (1993) Lysosomal accumulation of unesterified cholesterol in model macrophage foam cells. *J Biol Chem* 268:9653–9660.
- Tabas I, Rosoff WJ, Boykow GC (1988) Acyl coenzyme A:cholesterol acyl transferase in macrophages utilizes a cellular pool of cholesterol oxidase-accessible cholesterol as substrate. *J Biol Chem* 263:1266–1272.
- Brasaemle DL, Attie AD (1990) Rapid intracellular transport of LDL-derived cholesterol to the plasma membrane in cultured fibroblasts. *J Lipid Res* 31:103–112.
- Liscum L, Munn NJ (1999) Intracellular cholesterol transport. *Biochim Biophys Acta* 1438:19–37.
- Kellner-Weibel G, et al. (1999) Crystallization of free cholesterol in model macrophage foam cells. *Arterioscler Thromb Vasc Biol* 19:1891–1898.
- Tangirala RK, et al. (1994) Formation of cholesterol monohydrate crystals in macrophage-derived foam cells. *J Lipid Res* 35:93–104.
- Kellner-Weibel G, et al. (1998) Effects of intracellular free cholesterol accumulation on macrophage viability: A model for foam cell death. *Arterioscler Thromb Vasc Biol* 18:423–431.
- Rajamäki K, et al. (2010) Cholesterol crystals activate the NLRP3 inflammasome in human macrophages: A novel link between cholesterol metabolism and inflammation. *PLoS One* 5:e11765.
- Abela GS (2010) Cholesterol crystals piercing the arterial plaque and intima trigger local and systemic inflammation. *J Clin Lipidol* 4:156–164.
- Nakamura H, Ohtsubo K (1992) Ultrastructure appearance of atherosclerosis in human and experimentally-induced animal models. *Electron Microsc Rev* 5:129–170.
- Bocan TM, Schifani TA, Guyton JR (1986) Ultrastructure of the human aortic fibrolipid lesion. Formation of the atherosclerotic lipid-rich core. *Am J Pathol* 123:413–424.
- Baumer Y, et al. (2017) Hyperlipidemia-induced cholesterol crystal production by endothelial cells promotes atherogenesis. *Nat Commun* 8:1129.
- Kruth HS (1997) Cholesterol deposition in atherosclerotic lesions. *Cholesterol* (Springer, New York), pp 319–362.
- Small DM, Shipley GG (1974) Physical-chemical basis of lipid deposition in atherosclerosis. *Science* 185:222–229.
- Craven BM (1976) Crystal structure of cholesterol monohydrate. *Nature* 260:727–729.
- Katz SS, Shipley GG, Small DM (1976) Physical chemistry of the lipids of human atherosclerotic lesions. Demonstration of a lesion intermediate between fatty streaks and advanced plaques. *J Clin Invest* 58:200–211.
- Chung DS, Benedek GB, Konikoff FM, Donovan JM (1993) Elastic free energy of anisotropic helical ribbons as metastable intermediates in the crystallization of cholesterol. *Proc Natl Acad Sci USA* 90:11341–11345.
- Konikoff FM, Chung DS, Donovan JM, Small DM, Carey MC (1992) Filamentous, helical, and tubular microstructures during cholesterol crystallization from bile. Evidence that cholesterol does not nucleate classic monohydrate plates. *J Clin Invest* 90:1155–1160.
- Weihls D, et al. (2005) Biliary cholesterol crystallization characterized by single-crystal cryogenic electron diffraction. *J Lipid Res* 46:942–948.
- Loomis CR, Shipley GG, Small DM (1979) The phase behavior of hydrated cholesterol. *J Lipid Res* 20:525–535.
- Shieh HS, Hoard LG, Nordman CE (1977) Crystal structure of anhydrous cholesterol. *Nature* 267:287–289.
- Bogren H, Larsson K (1963) An X-ray-diffraction study of crystalline cholesterol in some pathological deposits in man. *Biochim Biophys Acta* 75:65–69.
- Solomonov I, Weygand MJ, Kjaer K, Rapaport H, Leiserowitz L (2005) Trapping crystal nucleation of cholesterol monohydrate: Relevance to pathological crystallization. *Biophys J* 88:1809–1817.
- Rapaport H, et al. (2001) Cholesterol monohydrate nucleation in ultrathin films on water. *Biophys J* 81:2729–2736.
- Ziblat R, Leiserowitz L, Addadi L (2011) Crystalline lipid domains: Characterization by X-ray diffraction and their relation to biology. *Angew Chem Int Ed Engl* 50:3620–3629.
- Ziblat R, Fargion I, Leiserowitz L, Addadi L (2012) Spontaneous formation of two-dimensional and three-dimensional cholesterol crystals in single hydrated lipid bilayers. *Biophys J* 103:255–264.
- Ong DS, et al. (2010) Extracellular cholesterol-rich microdomains generated by human macrophages and their potential function in reverse cholesterol transport. *J Lipid Res* 51:2303–2313.
- Varsano N, Fargion I, Wolf SG, Leiserowitz L, Addadi L (2015) Formation of 3D cholesterol crystals from 2D nucleation sites in lipid bilayer membranes: Implications for atherosclerosis. *J Am Chem Soc* 137:1601–1607.
- Varsano N, et al. (2016) Development of correlative cryo-soft X-ray tomography and stochastic reconstruction microscopy. A study of cholesterol crystal early formation in cells. *J Am Chem Soc* 138:14931–14940.
- Perl-Treves D, Kessler N, Izhaky D, Addadi L (1996) Monoclonal antibody recognition of cholesterol monohydrate crystal faces. *Chem Biol* 3:567–577.
- Addadi L, Rubin N, Scheffer L, Ziblat R (2008) Two and three-dimensional pattern recognition of organized surfaces by specific antibodies. *Acc Chem Res* 41:254–264.
- Kruth HS, et al. (2001) Monoclonal antibody detection of plasma membrane cholesterol microdomains responsive to cholesterol trafficking. *J Lipid Res* 42:1492–1500.
- Freeman SR, et al. (2014) ABCG1-mediated generation of extracellular cholesterol microdomains. *J Lipid Res* 55:115–127.
- Sorrentino A, et al. (2015) MISTRAL: A transmission soft X-ray microscopy beamline for cryo nano-tomography of biological samples and magnetic domains imaging. *J Synchrotron Radiat* 22:1112–1117.
- Jin S, et al. (2007) Structure of macroscopic monodomains and its soft confinements of chiral smectic phases on crystallization in a main-chain nonracemic liquid crystalline polyester. *Macromolecules* 40:5450–5459.
- Nakashima N, Asakuma S, Kunitake T (1985) Optical microscopic study of helical superstructures of chiral bilayer membranes. *J Am Chem Soc* 107:509–510.
- Shtukenberg A, et al. (2011) Bernauer's bands. *ChemPhysChem* 12:1558–1571.
- Shtukenberg AG, et al. (2012) Twisted mannitol crystals establish homologous growth mechanisms for high-polymer and small-molecule ring-banded spherulites. *J Am Chem Soc* 134:6354–6364.
- Shtukenberg AG, Punin YO, Gujral A, Kahr B (2014) Growth actuated bending and twisting of single crystals. *Angew Chem Int Ed Engl* 53:672–699.
- Konikoff FM, Cohen DE, Carey MC (1994) Phospholipid molecular species influence crystal habits and transition sequences of metastable intermediates during cholesterol crystallization from bile salt-rich model bile. *J Lipid Res* 35:60–70.
- van Meer G, Voelker DR, Feigenson GW (2008) Membrane lipids: Where they are and how they behave. *Nat Rev Mol Cell Biol* 9:112–124.
- Abela GS, et al. (2009) Effect of cholesterol crystals on plaques and intima in arteries of patients with acute coronary and cerebrovascular syndromes. *Am J Cardiol* 103:959–968.
- Ghidoni JJ, O'Neal RM (1967) Recent advances in molecular pathology: A review ultrastructure of human atheroma. *Exp Mol Pathol* 7:378–400.